Optics Letters

Temporal Talbot effect in free space

Layton A. Hall,[1] Sergey Ponomarenko,[2,3] and Ayman F. Abouraddy[1,*]

[1]CREOL, The College of Optics & Photonics, University of Central Florida, Orlando, Florida 32816, USA
[2]Department of Electrical and Computer Engineering, Dalhousie University, Halifax, Nova Scotia B3J 2X4, Canada
[3]Department of Physics and Atmospheric Science, Dalhousie University, Halifax, Nova Scotia B3H 4R2, Canada
*Corresponding author: raddy@creol.ucf.edu

Received 22 March 2021; revised 29 April 2021; accepted 30 April 2021; posted 3 May 2021 (Doc. ID 425635); published 23 June 2021

The temporal Talbot effect refers to the periodic revivals of a pulse train propagating in a dispersive medium and is a temporal analog of the spatial Talbot effect with group-velocity dispersion in time replacing diffraction in space. Because of typically large temporal Talbot lengths, this effect has been observed to date in only single-mode fibers, rather than with freely propagating fields in bulk dispersive media. Here we demonstrate for the first time, to the best of our knowledge, the temporal Talbot effect in free space by employing dispersive space-time wave packets, whose spatiotemporal structure induces group-velocity dispersion of controllable magnitude and sign in free space.

https://doi.org/10.1364/OL.425635

The Talbot effect, reported for the first time in 1836 [1], refers to the axial revivals of an initially periodic transverse spatial field structure [2]. This fascinating phenomenon has found a broad range of applications, spanning structured illumination in fluorescence microscopy [3–5] to prime-number decomposition [6], and phase-locking of laser arrays [7]. In an analogous *temporal* Talbot effect, whereupon group-velocity dispersion (GVD) in time replaces diffraction in space [8,9], a periodic pulse train of period T traveling in a dispersive medium undergoes periodic revivals at multiples of the temporal Talbot distance $z_T = \frac{T^2}{\pi|k_2|}$, where k_2 is the GVD parameter [9]. This effect was proposed in [10], demonstrated experimentally in [11] (and subsequently in [12,13]), and has been used in removing pulse distortion [14], pulse-rate multiplication [12,15], and pulse compression [16].

The temporal Talbot effect has yet to be observed in a freely propagating optical field. Because dispersion lengths for typical pulse trains are usually very large, the temporal Talbot effect has been instead realized only in single-mode fibers (z_T on the order of kilometers, with $k_2 \approx -26\ \mathrm{fs}^2/\mathrm{mm}$ at 1500 nm) [11] or in fiber Bragg gratings with higher GVD [14] (z_T on the order of tens of centimeters with $k_2 \approx -10^5\ \mathrm{fs}^2/\mathrm{mm}$) [Fig. 1(a)], but *not* in dispersive bulk media where diffraction that unavoidably accompanies propagation hampers its observation.

Here we demonstrate—for the first time to the best of our knowledge—the temporal Talbot effect in a freely propagating field over short distances (a few centimeters) *in free space*, without resort to any dispersive medium [Fig. 1(b)]. This surprising effect is made possible by exploiting dispersive "space-time" (ST) wave packets [17]. In general, ST wave packets [18–20] are pulsed beams endowed with a precise spatiotemporal structure [21–23] inculcating angular dispersion [24,25], by virtue of which they display a variety of unique behaviors, including propagation invariance [26–31], tunable group velocities in absence of dispersion [32–34], self-healing [35], and free-space acceleration/deceleration [36–39], among many other possibilities [40–42]. Rather than propagation-invariant ST wave packets, observing the temporal Talbot effect requires utilizing their counterparts exhibiting GVD in free space [17]. Because the angular dispersion underpinning ST wave packets is non-differentiable [43], unlike conventional angular dispersion associated with tilted pulse fronts (TPFs) that is differentiable [24,25], ST wave packets can experience arbitrary GVD in free space [17] whereas TPFs can experience only anomalous GVD [24,25,44]. After introducing normal or anomalous GVD of large magnitude, periodically sampling the temporal spectrum of the ST wave packet produces the temporal Talbot effect with

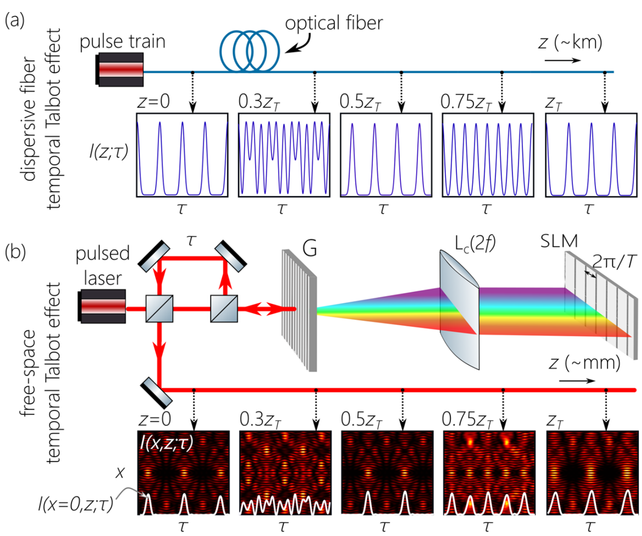

Fig. 1. (a) Temporal Talbot effect for a periodic pulse train manifested in axial revivals along a dispersive optical fiber. The plots are the intensity $I(z;\tau)$ along z; z_T is the temporal Talbot length. (b) Temporal Talbot effect realized in free space via dispersive ST wave packets. Schematic of the setup: G, diffraction grating; L_c, cylindrical lens; SLM, spatial light modulator. The panels display the spatiotemporal intensity $I(x,z;\tau)$ at different z, and the white curves are the on-axis profiles $I(0,z;\tau)$, which are identical to $I(z;\tau)$ in (a).

z_T on the order of a few centimeters (≈ 2 cm here). Crucially, because the spatial and temporal degrees of freedom are coupled, the initial (non-periodic) spatial profile is repeated at the temporal Talbot planes, thereby facilitating unambiguous observation of on-axis temporal revivals in free space for the first time.

We start by describing propagation-invariant ST wave packets in which each spatial frequency k_x is associated with a single temporal frequency ω to ensure that the axial wavenumber k_z is related linearly to ω, $\Omega = (k_z - k_o)c \tan\theta$; here $\Omega = \omega - \omega_o$ is the temporal frequency relative to a fixed frequency ω_o, $k_o = \frac{\omega_o}{c}$ is the corresponding wavenumber, c is the speed of light in vacuum, x and z are the transverse and longitudinal coordinates, respectively, the field is held uniform along y for simplicity, and we refer to θ as the spectral tilt angle. Geometrically, this construction is equivalent to restricting the spatiotemporal spectrum on the surface of the light-cone $k_x^2 + k_z^2 = (\frac{\omega}{c})^2$ to its intersection with a plane that is parallel to the k_x axis and is tilted by an angle θ with respect to the k_z axis, such that its projection onto the $(k_z, \frac{\omega}{c})$ plane is the straight line $k_z = k_o + \frac{\Omega}{c}\cot\theta$. Such a ST wave packet is propagation-invariant $\psi(x, z; t) = \psi(x, 0; t - z/\tilde{v})$, where $\psi(x, z; t)$ is the spatiotemporal envelope of the field $E(x, z; t) = e^{i(k_o z - \omega_o t)}\psi(x, z; t)$, and $\tilde{v} = c \tan\theta$ is the group velocity [26]. By replacing the plane with a planar curved surface that is also parallel to the k_x axis but whose projection onto the $(k_z, \frac{\omega}{c})$ plane is the curve $k_z = k_o + \Omega/\tilde{v} + k_2\Omega^2/2$, then the envelope takes the following form:

$$\psi(x, z; t) = \int d\Omega \tilde{\psi}(\Omega) e^{ik_x(\Omega)x} e^{-i\Omega(t - z/\tilde{v})} e^{ik_2\Omega^2 z/2}. \quad \text{(1)}$$

The on-axis envelope $\psi(0, z; t)$ takes the form of a plane wave pulse undergoing GVD (with GVD parameter k_2) along z, albeit in absence of a dispersive medium.

We introduce a periodic pulse train structure into the field by discretizing the temporal spectrum along ω at multiples of $\frac{2\pi}{T}$, $\Omega \to \Omega_m = m\frac{2\pi}{T}$ for integer m, so that the on-axis envelope is

$$\psi(0, z; t) = \sum_m \tilde{\psi}_m e^{-i2\pi m(t - z/\tilde{v})/T} e^{i2\pi\,\mathrm{sgn}(k_2) m^2 z/z_T}, \quad \text{(2)}$$

where $\mathrm{sgn}(k_2) = \pm 1$ is the sign of k_2, $\tilde{\psi}_m = \tilde{\psi}(\Omega_m)$ and $z_T = T^2/\pi|k_2|$. The tight association between temporal and spatial frequencies entails simultaneously discretizing the spatial spectrum along k_x. However, because ω and k_x are *not* linearly related, k_x is, therefore, *not* sampled periodically, and the transverse spatial profile at $z = 0$ is, thus, not periodic. The initial envelope is periodic in time $\psi(0, 0; t + \ell T) = \psi(0, 0; t)$ and is axially revived at the Talbot planes $\psi(0, \ell z_T; t) = \psi(0, 0; t - \ell z/\tilde{v})$ in a time frame traveling at $\tilde{v}$.

We prepare the ST field using the 2D pulse synthesizer developed in [26,32–34] and shown schematically in Fig. 1(b). This arrangement implements a two-step spatiotemporal spectral synthesis strategy capable of producing arbitrary, non-differentiable angular dispersion [17,45,46]. Plane wave pulses (pulse width $\sim$100 fs at a central wavelength $\sim$800 nm) from a mode-locked Ti:sapphire laser (Tsunami; Spectra Physics) are directed to a diffraction grating that spreads the pulse spectrum in space, whereupon the first diffraction order is collimated with a cylindrical lens before impinging on a reflective, phase-only spatial light modulator (SLM). The SLM imparts a 2D phase distribution to the spectrally resolved wavefront that assigns to each wavelength λ a spatial frequency $k_x(\lambda)$ to guarantee that $k_z(\Omega, k_x) = k_o + \Omega/\tilde{v} + k_2\Omega^2/2$, for given $\tilde{v}$ and k_2. The retro-reflected field returns to the grating whereupon the ST wave packets are reconstituted with an on-axis pulse width of ≈ 2 ps. We measure the spatiotemporal spectrum via a combination of a grating and a lens to carry out temporal and spatial Fourier transforms, and we obtain the spatiotemporal intensity profile by interfering the ST field with a short plane wave reference pulse from the Ti:sapphire laser [32,34].

We plot in Fig. 2 the measured spatiotemporal spectra for dispersive ST wave packets. In Fig. 2(a), we plot the spectral projections onto the (k_x, λ) and (k_z, λ) planes for normal GVD whereupon the spectral projection onto the (k_x, λ) plane is O-shaped. The GVD parameter here is $k_2 = 10^6$ fs^2/mm, which is significantly larger than ZnSe $k_2 \approx 10^3$ fs^2/mm (at $\lambda = 800$ nm) and Bragg gratings ($k_2 \approx 10^5$ fs^2/mm). Once the temporal spectrum is discretized [Fig. 2(b)] to produce a period $T = 8$ ps, an on-axis ($x = 0$) periodic pulse train structure emerges with a predicted temporal Talbot length of $z_T \approx 20$ mm because of the rapidly dispersing wave packet.

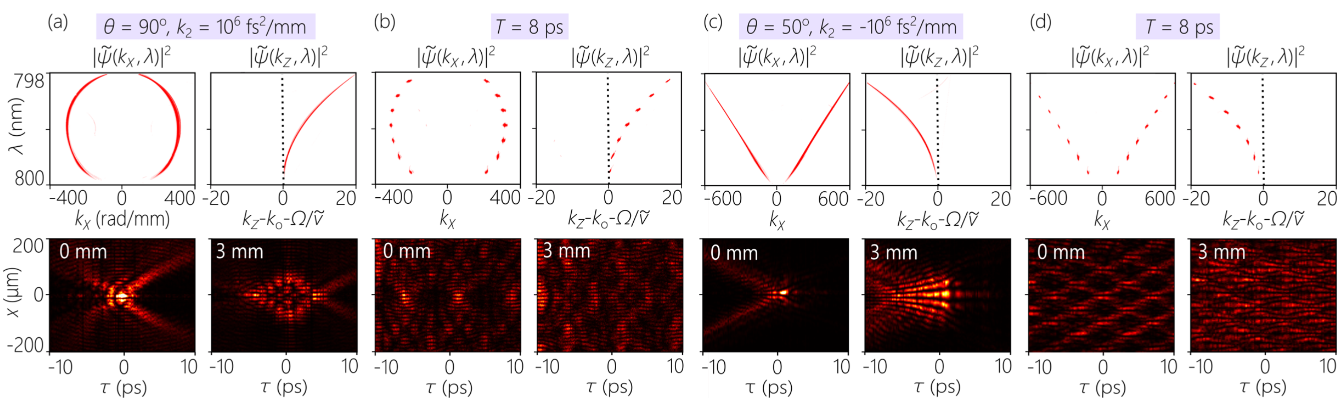

Fig. 2. First row shows continuous and discretized spectral projections onto the (k_x, λ) and (k_z, λ) planes, $|\tilde{\psi}(k_x, \lambda)|^2$ and $|\tilde{\psi}(k_z, \lambda)|^2$, respectively, for dispersive ST wave packets. The second row shows the spatiotemporal intensity profiles at $z = 0$ and $z = 3$ mm for each wave packet. The dotted vertical line in the spectral projection onto the (k_z, λ) plane corresponds to a GVD-free ST wave packet. (a) Dispersive ST wave packet having $\theta = 50°$ and normal $k_2 = 10^6$ fs^2/mm. (b) Same as (a) after discretizing the spectrum to produce a pulse train of period $T = 8$ ps. (c), (d) Same as (a), (b), except for $\theta = 90°$ and anomalous GVD $k_2 = -10^6$ fs^2/mm.

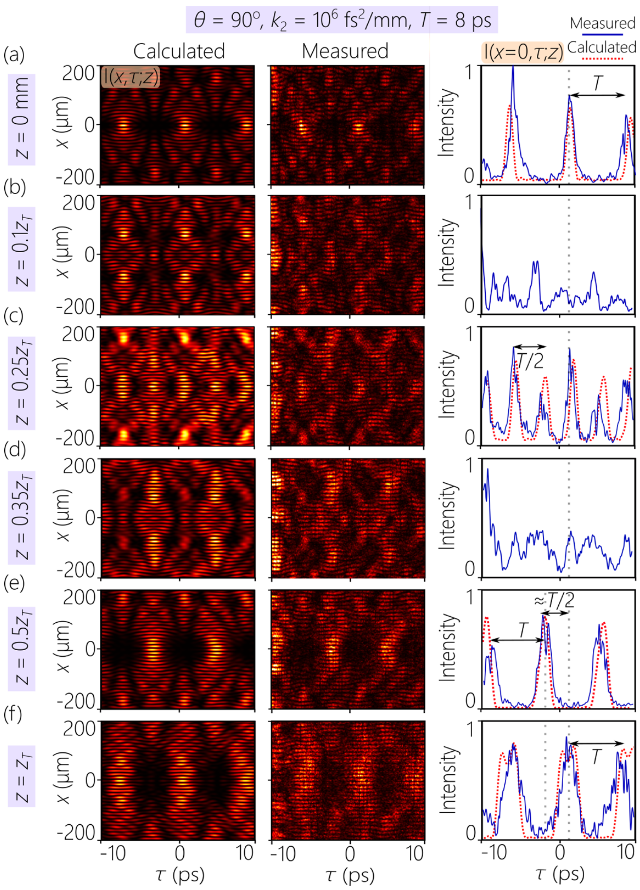

Fig. 3. Demonstration of the temporal Talbot effect in free space employing the dispersive ST wave packet experiencing normal dispersion in free space from Fig. 2(b).

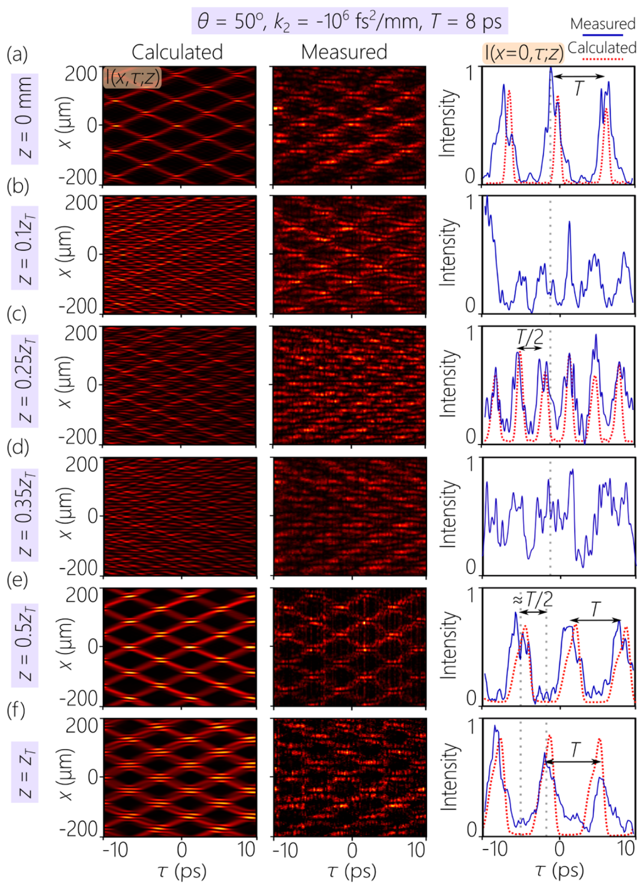

Fig. 4. Demonstration of the temporal Talbot effect in free space employing the dispersive ST wave packet experiencing anomalous dispersion in free space from Fig. 2(d).

We plot in Fig. 2(c) the measured spatiotemporal spectral projections onto the (k_x, λ) and (k_z, λ) planes after introducing anomalous GVD equal in magnitude but opposite in sign to that in Fig. 2(a). We plot in Fig. 2(d) the corresponding profiles after spectral discretization with $T = 8$ ps.

Despite the clear distinction between the profiles for normally dispersive ST fields with continuous and discretized spectra [Figs. 2(a), 2(b)] and their anomalously dispersive counterparts [Figs. 2(c), 2(d)], the on-axis intensity in both are nevertheless similar [Eq. (1)] with both exhibiting axial revivals of the initial periodic temporal profile. The measurement results for axial propagation of the dispersive ST wave packets alongside theoretical predictions are presented in Fig. 3 for normal GVD corresponding to Fig. 2(b), and in Fig. 4 for anomalous GVD corresponding to Fig. 2(d), both with $T = 8$ ps. We measure the temporally resolved intensity at the axial planes $z = 0$, $0.1z_{\mathrm{T}}$, $0.25z_{\mathrm{T}}$, $0.35z_{\mathrm{T}}$, $0.5z_{\mathrm{T}}$, and z_{T}. There is excellent agreement between the calculated (first column) and measured (second column) intensity profiles. The on-axis temporal profiles (third column) reveal several critical features. First, the initial period profile [Figs. 3(a) and 4(a)] is retrieved at the Talbot planes $z = mz_{\mathrm{T}}$ [Figs. 3(f) and 4(f)]. Second, the periodic profile is reconstructed at the Talbot half-planes $z = (m + \frac{1}{2})z_{\mathrm{T}}$ but with a temporal displacement by $T/2$ with respect to $z = mz_{\mathrm{T}}$ [Figs. 3(e) and 4(e)]. Third, at $z = 0.25z_{\mathrm{T}}$, a rate doubling is observed, i.e., a periodic profile is observed but with period $T/2$ rather than T [Figs. 3(c) and 4(c)]. We repeat the measurements for different values of the GVD parameter k_2 and obtain the temporal Talbot length z_{T}. The data plotted in Fig. 5(a) show excellent agreement with the theoretical expectation of $z_{\mathrm{T}} = \frac{T^2}{\pi|k_2|}$ with $T = 8$ ps.

We recently reported a phenomenon we denoted the "veiled" Talbot effect resulting from periodically sampling the spatial spectrum along k_x for a *propagation-invariant* ST wave packet [47]. The conventional spatial Talbot effect was observed in time-resolved measurements as a consequence of time diffraction [27,48–50], but no temporal dynamics are observed in absence of GVD. The time-averaged intensity (or energy) is diffraction-free along z with a period $L/2$ rather than L. In the work reported here, the transverse profile is *not* periodic, and yet the time-averaged intensity remains diffraction-free, as shown in Fig. 5(b) for normal and anomalous GVD, despite the underlying axial dynamics (Figs. 3 and 4).

We have also reported on a ST Talbot effect based on the unique dispersive ST wave packet denoted a "V-wave" whose diffraction and dispersion lengths are intrinsically equal [51]. Because k_x and ω are linearly related in a V-wave, k_x and ω can be simultaneously sampled periodically to guarantee equal spatial and temporal Talbot lengths. However, this is a restrictive condition that admits of this unique solution. The Talbot effect we present here is purely temporal. Crucially, V-waves are endowed with differentiable angular dispersion, so they are

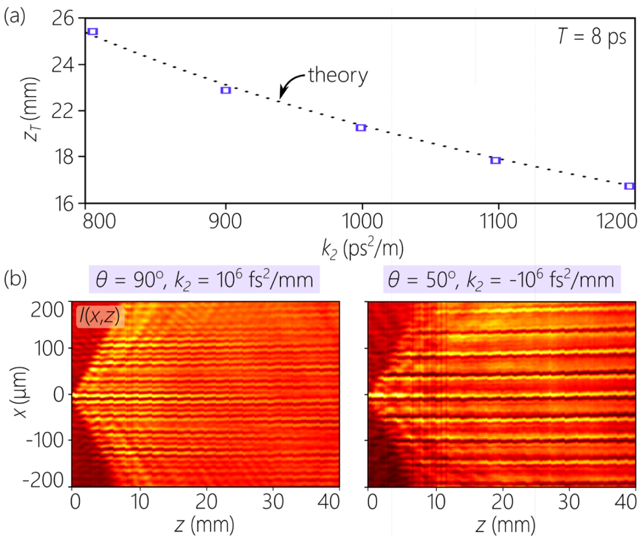

Fig. 5. (a) Measured temporal Talbot length z_T while varying the GVD parameter in the normal regime. The dotted curve is $z_T = T^2/(\pi|k_2|)$. (b) Time-averaged intensity $I(x, z)$ for both normal and anomalous GVD, showing axial invariance despite the underlying temporal evolution (Fig. 3 and Fig. 4).

amenable to the conventional perturbative theory [44]; they, therefore, can inculcate only anomalous GVD. In contrast, non-differentiable angular dispersion introduced here [43] produces either normal or anomalous GVD [17].

In conclusion, we have observed for the first time the temporal Talbot effect with a freely propagating field rather than a confined mode in a single-mode fiber. This demonstration made use of dispersive ST wave packets undergirded by non-differentiable angular dispersion that allows us to induce in free space normal or anomalous GVD of extremely large magnitudes, thus reducing the temporal Talbot length to $z_T \sim 20$ mm. Moreover, the initial non-periodic *spatial* profile is simultaneously revived at the *temporal* Talbot planes, thereby allowing for the unambiguous observation of this effect.

Funding. Office of Naval Research (N00014-17-1-2458, N00014-20-1-2789).

Disclosures. The authors declare no conflicts of interest.

Data Availability. Data underlying the results presented in this paper are not publicly available at this time but may be obtained from the authors upon reasonable request.

REFERENCES

1. H. F. Talbot, Philos. Mag. **9**, 401 (1836).
2. J. Wen, Y. Zhang, and M. Xiao, Adv. Opt. Photon. **5**, 83 (2013).
3. C. Han, S. Pang, D. V. Bower, P. Yiu, and C. Yang, Anal. Chem. **85**, 2356 (2013).
4. Y. Sun and S. Pang, J. Biomed. Opt. **21**, 086003 (2016).
5. S. Chowdhury, J. Chen, and J. A. Izatt, "Structured illumination fluorescence microscopy using Talbot self-imaging effect for high-throughput visualization," arXiv:1801.03540 (2018).
6. K. Pelka, J. Graf, T. Mehringer, and J. von Zanthier, Opt. Express **26**, 15009 (2018).
7. C. Tradonsky, V. Pal, R. Chriki, N. Davidson, and A. A. Friesem, Appl. Opt. **56**, A126 (2017).
8. B. H. Kolner, IEEE J. Quantum Electron. **30**, 1951 (1994).
9. F. Mitschke and U. Morgner, Opt. Photon. News **9**, 45 (1998).
10. T. Jannson and J. Jannson, J. Opt. Soc. Am. **71**, 1373 (1981).
11. P. A. Andrekson, Opt. Lett. **18**, 1621 (1993).
12. S. Arahira, S. Kutsuzawa, Y. Matsui, D. Kunimatsu, and Y. Ogawa, J. Light. Technol. **16**, 405 (1998).
13. I. Shake, H. Takara, S. Kawanishi, and M. Saruwatari, Electron. Lett. **34**, 792 (1998).
14. J. Azaña and M. A. Muriel, Appl. Opt. **38**, 6700 (1999).
15. S. Atkins and B. Fischer, IEEE Photon. Technol. Lett. **15**, 132 (2003).
16. N. K. Berger, B. Levit, A. Bekker, and B. Fischer, IEEE Photon. Technol. Lett. **16**, 1855 (2004).
17. M. Yessenov, L. A. Hall, and A. F. Abouraddy, "Engineering the optical vacuum: arbitrary magnitude, sign, and order of dispersion in free space using space-time wave packets," arXiv:2102.09443 (2021).
18. H. E. Kondakci and A. F. Abouraddy, Opt. Express **24**, 28659 (2016).
19. K. J. Parker and M. A. Alonso, Opt. Express **24**, 28669 (2016).
20. M. Yessenov, B. Bhaduri, H. E. Kondakci, and A. F. Abouraddy, Opt. Photon. News **30**, 34 (2019).
21. J. Turunen and A. T. Friberg, Prog. Opt. **54**, 1 (2010).
22. K. Reivelt and P. Saari, "Localized wave solutions of the scalar homogeneous wave equation and their optical implementation," arxiv:physics/0309079 (2003).
23. H. E. Hernández-Figueroa, E. Recami, and M. Zamboni-Rached, eds., *Non-Diffracting Waves* (Wiley-VCH, 2014).
24. J. P. Torres, M. Hendrych, and A. Valencia, Adv. Opt. Photon. **2**, 319 (2010).
25. J. A. Fülöp and J. Hebling, in *Recent Optical and Photonic Technologies*, K. Y. Kim, ed. (InTech, 2010).
26. H. E. Kondakci and A. F. Abouraddy, Nat. Photon. **11**, 733 (2017).
27. H. E. Kondakci and A. F. Abouraddy, Phys. Rev. Lett. **120**, 163901 (2018).
28. B. Bhaduri, M. Yessenov, D. Reyes, J. Pena, M. Meem, S. R. Fairchild, R. Menon, M. C. Richardson, and A. F. Abouraddy, Opt. Lett. **44**, 2073 (2019).
29. K. L. Schepler, M. Yessenov, Y. Zhiyenbayev, and A. F. Abouraddy, ACS Photon. **7**, 2966 (2020).
30. A. Shiri, M. Yessenov, S. Webster, K. L. Schepler, and A. F. Abouraddy, Nat. Commun. **11**, 6273 (2020).
31. A. Shiri, M. Yessenov, R. Aravindakshan, and A. F. Abouraddy, Opt. Lett. **45**, 1774 (2020).
32. H. E. Kondakci and A. F. Abouraddy, Nat. Commun. **10**, 929 (2019).
33. B. Bhaduri, M. Yessenov, and A. F. Abouraddy, Optica **6**, 139 (2019).
34. B. Bhaduri, M. Yessenov, and A. F. Abouraddy, Nat. Photon. **14**, 416 (2020).
35. H. E. Kondakci and A. F. Abouraddy, Opt. Lett. **43**, 3830 (2018).
36. M. Clerici, D. Faccio, A. Lotti, E. Rubino, O. Jedrkiewicz, J. Biegert, and P. D. Trapani, Opt. Express **16**, 19807 (2008).
37. H. Valtna-Lukner, P. Bowlan, M. Lõhmus, P. Piksarv, R. Trebino, and P. Saari, Opt. Express **17**, 14948 (2009).
38. M. Yessenov and A. F. Abouraddy, Phys. Rev. Lett. **125**, 233901 (2020).
39. Z. Li and J. Kawanaka, Commun. Phys. **3**, 211 (2020).
40. L. J. Wong and I. Kaminer, ACS Photon. **4**, 2257 (2017).
41. A. M. Shaltout, K. G. Lagoudakis, J. van de Groep, S. J. Kim, J. Vučković, V. M. Shalaev, and M. L. Brongersma, Science **365**, 374 (2019).
42. A. Chong, C. Wan, J. Chen, and Q. Zhan, Nat. Photon. **14**, 350 (2020).
43. L. A. Hall, M. Yessenov, and A. F. Abouraddy, Opt. Lett. **46**, 1672 (2021).
44. O. E. Martinez, J. P. Gordon, and R. L. Fork, J. Opt. Soc. Am. A **1**, 1003 (1984).
45. M. Yessenov, B. Bhaduri, L. Mach, D. Mardani, H. E. Kondakci, M. A. Alonso, G. A. Atia, and A. F. Abouraddy, Opt. Express **27**, 12443 (2019).
46. H. E. Kondakci, N. S. Nye, D. N. Christodoulides, and A. F. Abouraddy, ACS Photon. **6**, 475 (2019).
47. M. Yessenov, L. A. Hall, S. A. Ponomarenko, and A. F. Abouraddy, Phys. Rev. Lett. **125**, 243901 (2020).
48. M. Moshinsky, Phys. Rev. **88**, 625 (1952).
49. S. Longhi, Opt. Express **12**, 935 (2004).
50. M. A. Porras, Opt. Lett. **42**, 4679 (2017).
51. L. A. Hall, M. Yessenov, S. A. Ponomarenko, and A. F. Abouraddy, It is clear that the initialAPL Photonics **6**, 056105 (2021).